Spacelab 1 Experiments on Interactions of an Energetic Electron Beam with Neutral Gas

J. A. Marshall,* C. S. Lin,† and J. L. Burch‡
Southwest Research Institute, San Antonio, Texas
T. Obayashi§
Institute of Space and Astronautical Science, Tokyo, Japan
and
C. Beghin¶
Laboratoire de Physique et Chimie de l'Environment, Orleans, France

An unusual signature of return current and spacecraft charging potential was observed during the Spacelab 1 mission launched on November 28, 1983. The phenomenon occurred during neutral gas releases from the SEPAC (Space Experiments with Particle Accelerators) magnetoplasma-dynamic arcjet (MPD) concurrent with firings of the PICPAB (Phenomena Induced by Charged Particle Beams) electron gun and was recorded by the instruments of the SEPAC diagnostic package (DGP). Data from the langmuir probe, floating probes, neutral gas pressure gauge, and the plasma wave probes are reported. As the dense neutral gas was released, the return current measured by the langmuir probe changed from positive to negative and a positive potential relative to the spacecraft was measured by the floating probe. The anomalous return current is believed to be attributable to secondary electron fluxes escaping from the spacecraft, and the unusual charging situation is attributed to the formation of a double-layer structure between a hot plasma cloud localized to the MPD and the spacecraft. The charging scenario is supported by a computer simulation.

Introduction

SPACELAB 1, which was flown for 10 days beginning on November 28, 1983, contained two active particle beam experiments: Space Experiments with Particle Accelerators (SEPAC)[1] and Phenomena Induced by Charged Particle beams (PICPAB).[2] The SEPAC experiment included an electron accelerator (the EBA), a plasma injector (a magnetoplasma-dynamic arcjet known as the MPD), and a neutral gas injector (a neutral gas plume known as the NGP), whereas the PICPAB experiment included an array of ion and electron accelerators. Both experiments were equipped with plasma diagnostic instruments. Detailed descriptions of SEPAC and PICPAB experiments can be found in Refs. 1 and 2. These two experiments were intended, in part, to study the interaction of beams with plasmas and neutral gas in space and the effects of beam emission on spacecraft charging. Some results from both experiments have been reported in the literature on plasma energization,[3] energy broadening due to space charge oscillations,[4] VLF and ELF wave phenomena,[5,6] and spacecraft charging.[7,8]

Experimental results from the interaction of a neutral nitrogen gas plume (from the SEPAC NGP) and one of the PICPAB electron beams indicate an occurrence of beam plasma discharge, or BPD[9]. During the observed BPD, a return current was measured by the langmuir probe as a sharp positive pulse, and intense optical emissions were simultaneously registered by the photometer. The experimental sequences under consideration here also involve the interaction of the PICPAB beam with a neutral gas. In this case, however, the gas is neutral Argon from the MPD. The data gathered by the SEPAC diagnostic package are quite different from those reported in Ref. 9, as the return current measured by the langmuir probe becomes negative in some cases, even though a positive voltage was applied to the probe. These data indicate an unusual spacecraft charging phenomenon that has not been reported before.

This report presents the results of a comprehensive analysis of all data available during releases of neutral gas from the MPD. Various causes of the negative current seen by the langmuir probe were evaluated. A plausible scenario was suggested to describe the behavior of the beam interacting with the neutral gas, and a computer simulation was then conducted to examine the scenario.

Description of the Experiment

The configuration of Spacelab 1 on the Shuttle pallet is shown in Fig. 1. The SEPAC diagnostic package (DGP) is located approximately 1 m from the PICPAB accelerators. The PICPAB electron beam, which was actually one of several charged particle beams associated with that experiment, was injected at a beam energy of 8 keV and a current of either 10 or 100 mA. All injections under consideration here were at 100 mA.

During standard operation, the SEPAC MPD releases 1 ms pulses of 10^{19} Argon ion-electron pairs (A^+/e^-). Neutral Argon gas is released from a chamber by a fast-acting valve so that it reaches a discharge electrode precisely at the moment of discharge. At the beginning of each experiment sequence (known as a functional objective or FO) involving the MPD, the chamber is filled to 2 atm, and then halfway through the FO, the pressure is increased to 3 atm. Before each pressurization, any gas remaining in the chamber must be released to ensure an accurate pressure. The amount of gas released in this manner is variable, depending on the amount of time elapsed since the chamber was last filled, because gas is constantly lost to leakage. In general, a much greater amount of gas remains to be released at the midpoint of the FO (only 2.5 min after the chamber was filled at the start) then at the beginning of an FO, which may be hours after the last pressurization.

The SEPAC DGP consisted of a langmuir probe, three floating probes, high- and low-frequency wave receivers, a vacuum gage, an energetic particle analyzer, and a photometer. A brief description of these diagnostic instruments follows.

Received Oct. 20, 1987; revision received May 9, 1988.

*Senior Research Scientist.
†Manager, Plasma Physics Section.
‡Vice President, Instrumentation and Space Research Division.
§Director, Space Plasma Division.
¶Professor.

The langmuir probe is designed to operate from −9V to +9V in either a swept or a fixed voltage mode. The langmuir probe samples current at 1 kHz and voltage at 250 Hz. In the fixed mode, used in conjunction with the accelerator firings discussed here, the probe measures electron densities from 10^4 to 10^8 cm^{-3}, but no temperature measurement is possible. The probe sensor is a gold-plated stainless steel cylinder 4 mm in diameter and 20 cm in length.

The three floating probe sensors are gold-plated cylinders 40 mm in diameter and 40 mm in length. They are separated vertically by a distance of 25 cm, with the lowest sensor 29 cm above the DGP mounting structure. These probes are capable of measuring potential differences between the ambient plasma and spacecraft ground from −8 kV to +8 kV. The top floating probe samples at 1 kHz, whereas the middle and bottom floating probes sample at 500 Hz.

The high-frequency wave sensor is a monopole antenna 30 mm in diameter and 435 mm in length. Mounted on top of the monopole antenna is a Faraday cup sensor monitoring low-frequency wave activity. The current to the Faraday cup and the potential induced on its outer shell are monitored. The frequency range is 100 kHz to 10 MHz for the high-frequency receiver and 750 Hz to 10 kHz for the low-frequency receiver.

The vacuum gage is capable of measuring neutral gas pressure from 5×10^{-4} to 5×10^{-8} Torr and was located at the base of the langmuir probe .

The energetic particle analyzer (EPA) consists of four pairs of deflection plates: three with channeltron detectors and one with a Faraday cup. The energy selected by the EPA was generally swept between 100 eV and 15 keV in FO's involving the SEPAC electron accelerator; but during the FO's under consideration here, the analyzer voltage was fixed at the 100 eV setting, making a measurement of the electron energy spectrum impossible.

The SEPAC photometer is mounted on a gimbal system capable of rotating ± 60 deg in one plane. It has a variable iris (9 deg to dark) and three filter settings: 3914, 5577, and 6300 Å. However, the usefulness of the photometer data was limited by the fact that all the experimental sequences discussed here occurred in sunlight, making it necessary to close the iris to its smallest diameter. Optical emissions like those discussed in Ref. 9 would have been difficult to register.

There was joint operation of the PICPAB electron beam with the SEPAC MPD during two functional objectives (FO8A and FO9B) and with the SEPAC NGP in two others (FO9A and FO6). Data from the NGP and PICPAB have been analyzed in Ref. 9, as mentioned in the introduction. The present article is mainly concerned with the data from FO8A and FO9B.

In FO8A, the Orbiter is oriented so as to make the velocity vector of the ions released by the MPD arcjet parallel to the magnetic field, minimizing deflection of the plasma jet. The arcjet is fired straight up from the payload bay. During the three performances of FO8A discussed here, the elevation component of the magnetic field varied from 90 to 135 deg in the orbiter coordinate system. During an FO9B sequence, the Orbiter is placed in an attitude so that the EBA will fire in the direction of local magnetic field lines, in the hope of maximizing beam propagation.

Results

Six times during the Spacelab 1 mission, neutral gas was released from the MPD (prior to a repressurization) while the PICPAB electron accelerator was firing. These six events divide themselves naturally into two classes according to the behavior of the langmuir probe during the release. The first class is characterized by a change in the way the langmuir probe registers the firing of the PICPAB beam: before the gas is released, the probe current shows a sharp positive peak with each beam pulse; during the release, on the other hand, the peaks become sharply negative. This class has four events occurring only in FO8A. In the second class of events, the langmuir probe current signature remains unchanged by the gas release, continuing to show a positive peak each time the beam is fired. This class has two events occurring in FO8A and FO9B. We first present data for the negative peak events.

Class 1: Negative Langmuir Probe Current

Figure 2 shows sample data starting from 03:37:0.5 Universal Time (UT) on December 7, 1983, for a 3 s interval. The FO8A sequence started 0.5 s before the start time of Fig. 2 and neutral Argon gas was released from the MPD at 03:37:0.9 UT. Signals from various diagnostic instruments are plotted as functions of time. This case is typical of the four events in that the behavior of the probes changes during the gas release. The occurrence of the gas release can clearly be seen on the top plot, which shows background neutral pressure as measured by the ionization gauge. Before the gas is released, the ambient neutral pressure is 3×10^{-6} Torr. After the release, the pressure increases by a factor of 23 (to 7×10^{-6} Torr) and then decreases steadily for about 2 s until it returns to the background level.

The current and voltage readings as a function of time for the langmuir probe are shown in the second and third panels (from the top) of the figure. In this case, as in all five events during FO8A, a constant +6V is applied to the langmuir probe (third panel). Prior to the neutral gas release, the PICPAB beam registers on the langmuir probe current trace as a 2 to 3 μA positive pulse once every 266 ms, corresponding to the frequency of accelerator firings. At 03:37:0.95 UT, the probe current pulses suddenly become negative, with an amplitude of −5 to −7 μA and the same frequency, corresponding to the first beam firing after the gas is released (second panel). After 03:37:2.0 UT, the neutral pressure falls below 10^{-5} Torr and the peaks become positive again.

The bottom two panels of Fig. 2 show the automatic gain control (AGC) readings for the low- (above) and high- (below) frequency wave probes. The firing of the PICPAB beam is seen on the low-frequency receiver as a decrease in gain (negative peak); the peak increases sharply in amplitude during the neutral Argon release, indicating an increase in wave activity (third panel). In this time interval, the effects of the electron beam on the high-frequency AGC can only be seen as a small negative peak during the first firing after the gas release (03:37:1.22 UT) and at 03:37:2.0 UT.

Figure 3 presents wave data from the low-frequency wave sensor for the same time interval as Fig. 2. The neutral pressure is shown again in the top panel for reference. The middle panel shows the scanning frequency, which varies during this time from 300 Hz to 8 kHz. The potential difference induced on the probe (in mV), which is proportional to the intensity of wave activity at the scanning frequency, is plotted in the bottom panel; the PICPAB beam firings can clearly be seen as peaks approximately four times a second. Before the increase in

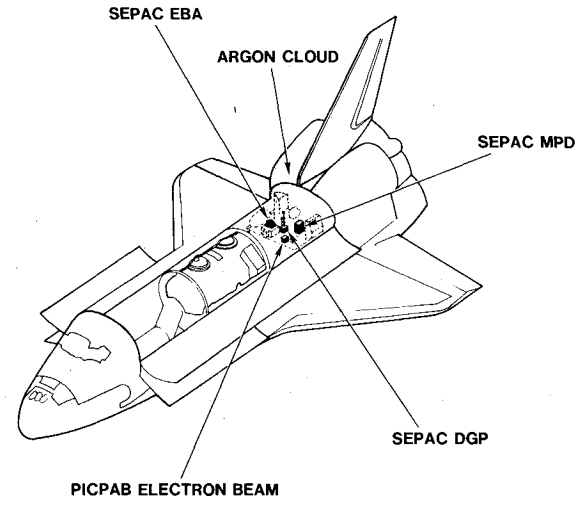

Fig. 1 Layout of the Spacelab 1 pallet. The PICPAB accelerator is approximately 1 m from the SEPAC gas injector module (containing the MPD) and 1 m from the SEPAC DGP.

neutral pressure, the peaks are 10–20 mV in height; while the neutral pressure is greater than 10^{-5} Torr (from 3:37:0.9 UT to 3:37:1.9 UT), the amplitude increases to 150 to 800 mV. The large amplitudes are detected when the scanning frequency varies from 1 to 6 kHz.

Recall that the complete range of the low-frequency probe is 100 Hz to 10 kHz. The high-frequency wave data from 100 kHz to 10 MHz do not show a clear pattern of wave activity corresponding to beam firings during the neutral Argon releases. In particular, there are no clear indications of the beam firings or possible wave emissions in the region of the electron plasma frequency (near 4 to 5 MHz). The apparent absence of electron plasma waves in the data could have been caused by the gain for the high-frequency receiver being set too low at this time.

In Fig. 3, the frequency is scanned from 1 to 6 kHz when the neutral pressure exceeds 10^{-5} Torr. In Fig. 4, we present a data set covering the remaining portions of the frequency range for an interval of elevated pressure level in the same format. The time interval of Fig. 4 is about 2 min later than that of Fig. 3. The induced potential once more shows peaks about four times a second corresponding to the PICPAB beam firings (bottom panel). Before the neutral gas release (and afterward), the induced voltage at each PICPAB firing is on the order of 30 to 50 mV. In this case, however, the amplitude of the peaks remains in the range of 40 to 100 mV while the probe scans frequency from 8 to 10 kHz (from 3:39:30.9 to 3:39:31.6 UT), even though the neutral pressure has increased above 10^{-5} Torr. From 3:39:31.7 to 3:39:32.3 UT, while the neutral pressure is still above 10^{-5} Torr and the scanning frequency varies from 500 Hz to 2 kHz, the peak height rises above the previous level, reaching 200 mV at 600 Hz and as high as 600 mV at 1 kHz. Figures 3 and 4 suggest that the wave activity during the elevated level of neutral gas pressure and beam firing is mainly limited to the 0.6 to 6 kHz frequency range.

From the peaks of induced potential voltage, we can construct an envelope plot of induced potential vs the scanning frequency, which describes quantitatively the wave spectrum in the frequency range of 0.1 to 10 kHz. The envelope plot corresponding to Fig. 3 is shown as a solid line in Fig. 5a, illustrating enhanced wave activities in the 1 to 6 kHz frequency range. The envelope for the sweep immediately following the neutral gas release is shown as a dashed line to indicate the level of activity without the additional neutral gas pressure. Figure 5b is a similar plot for the time period shown in Fig. 4. Recall that, in this case, the neutral gas was above the critical 10^{-5} Torr level while the probe was set to scan from 8 to 10 kHz and from 0.1 to 1 kHz. The significant increases above the scan at lower pressure (dotted line) are in the 0.6 to 1.0 kHz range.

Together, Figs. 5a and 5b reiterate that the wave activity measured by the low-frequency wave probe is concentrated in the 0.6 to 6 kHz range when the neutral pressure is elevated above 10^{-5} Torr. If the electron plasma frequency is much higher than the electron gyrofrequency, the lower hybrid resonance frequency for a single-ion plasma can be approximated by $\Omega_{LH} = eB/c\sqrt{M_i m_e}$ for the magnetic induction in the ionosphere B ($=0.3$ G), ion mass M_i, and electron mass m_e. Therefore, the lower hybrid resonance frequency for single-ion plasmas of N^+ (5.2 kHz), O^+ (4.9 kHz), and A^+ (3.1 kHz) all fall within this range.

Data from the three floating probe sensors are shown in the bottom three panels of Fig. 6 for the interval corresponding to Fig. 2. The top panel shows the neutral gas pressure (as in Fig. 2) as a time reference for the occurrence of the Argon release. The next three panels display successively the potential of the ambient plasma at the top, middle, and bottom floating probes relative to spacecraft ground. The floating probe data indicate a marked change during the gas release. Before the neutral gas is released, there is no indication of the beam firing in the floating probe voltage: the top probe shows a 5V noise signal and the middle and bottom probes no signal. When the neutral pressure is increased, all three sensors show sharp positive pulses about 7V in amplitude. Since the bottom probe is 27 cm

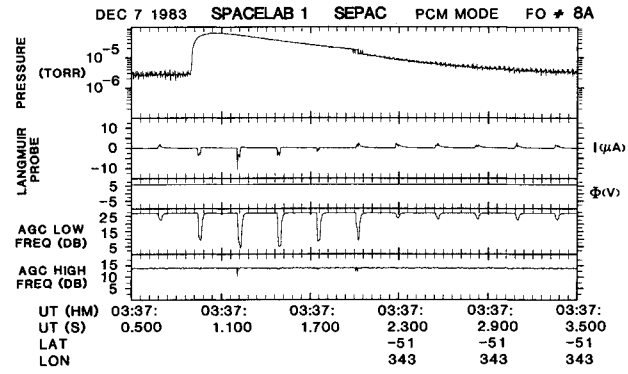

Fig. 2 Data acquired by the SEPAC DGP as a function of time (x axis). The panels show (from the top): the neutral pressure, langmuir probe current, voltage applied to the langmuir probe, and automatic gain control (AGC) readings for the low-frequency wave probe and high-frequency wave probe AGC. The Shuttle latitude (LAT) and longitude (LON) are shown at the bottom.

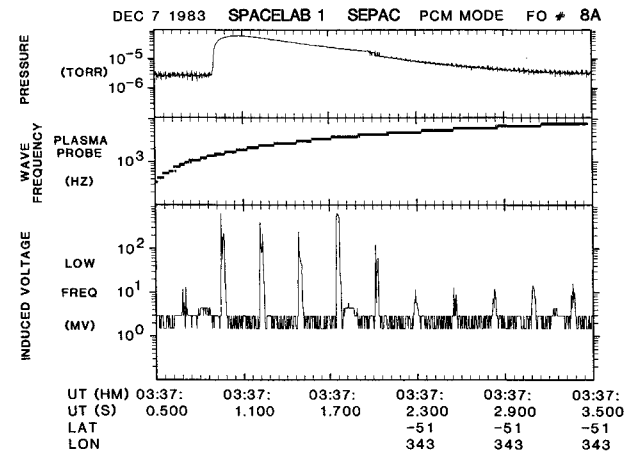

Fig. 3 Frequency (middle panel) and induced voltage (bottom panel) for the low-frequency wave probe sensor. The top panel shows the neutral pressure during the same time period.

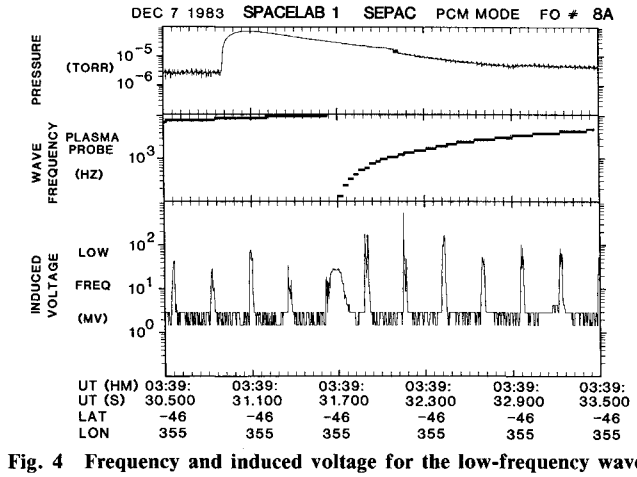

Fig. 4 Frequency and induced voltage for the low-frequency wave probe sensor.

above the Spacelab pallet, we estimate that the potential gradient is about 24 V/m between the bottom probe and the spacecraft and negligible above the bottom probe.

The floating probe measurements for the other three events in the group are similar to the event shown in Fig. 6, although the magnitudes of the potential gradient are different. One event (02:24:30–33 UT on December 7, 1983) has floating probe behavior identical to that shown in Fig. 6. In another case

(02:54:31-33 UT on December 7, 1983), the potential gradient is unclear because dense noise obscures the characteristic on the top probe, and the middle and bottom sensors show no induced voltage. Finally, the event corresponding to the interval of Fig. 4 is illustrated in Fig. 7. The middle probe actually shows small negative voltage peaks corresponding to beam firings before the gas release and large positive voltage peaks about +20V during the high gas pressure (third panel). The top probe measured +25V peaks and the bottom probe +15V peaks while the additional gas was present. In this case, the electric field is estimated to be about 45 V/m between the bottom probe and the spacecraft.

As just mentioned, the EPA voltage was set to detect only electrons with energies in a narrow passband around 100 eV. In all four of the class 1 examples, the EPA shows some energy flux enhancement (sometimes as high as 10^9 eV/cm^2-sr-s-keV over the background level of 5×10^7 eV/cm^2-sr-s-keV) coincident with the PICPAB beam firings. In one instance, December 7, 1983 from 2:24:30 until 2:24:33 UT, there is significant continued enhancement during the neutral gas release. After the neutral gas is released (at 2:24:30.9 UT), the energy flux between firings remains above background level, at greater than 3×10^8 eV/cm^2-sr-s-keV, indicating the existence of an electron cloud whose temperature is at least 100 eV.

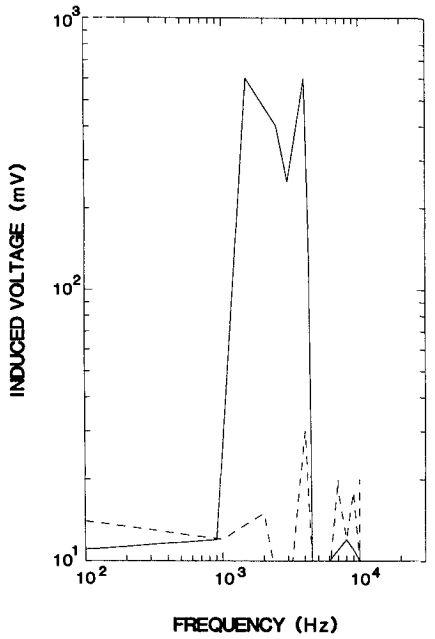

Fig. 5a Envelope plots of induced voltage vs frequency from the data shown in Fig. 3.

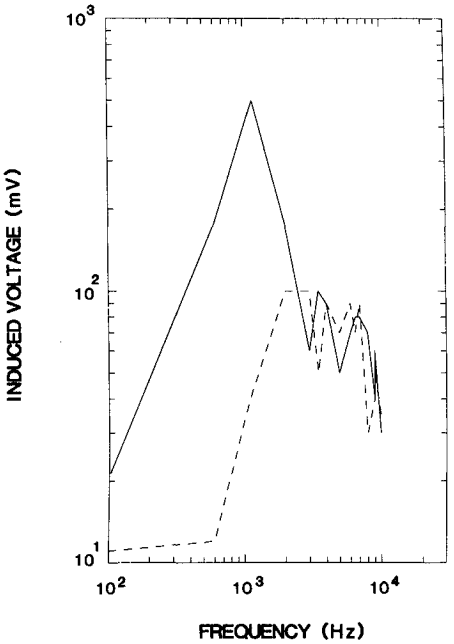

Fig. 5b Envelope plots of induced voltage vs frequency from the data shown in Fig. 4.

Class 2: Positive Langmuir Probe Current

The second class of events, in which the probe current remains positive during the gas release, has two events. One example is illustrated in Fig. 8. This event started at 02:52:1.1 UT, near the beginning of the FO8A, which was performed approximately 25 min after the last FO involving the MPD. The top plot shows that the neutral pressure increases only by a factor of six. (Recall that the neutral gas pressure increases by a factor of 23 in the first class of events discussed here.) The lower plots show that there is no change in the signals from the langmuir probe (second and third panel), the floating probes (fourth panel), or the wave probe AGC's (fifth and bottom panels), concurrent with PICPAB accelerator firings during the neutral Argon release from the MPD. The EPA data from this event (not shown) give no indication of the beam firings or the neutral gas release. The other event in this class, which occurred during the period from 18:48:01 to 18:48:04 UT on December 4, 1983, is similar in character to the case in FO8A just discussed so the data are not shown.

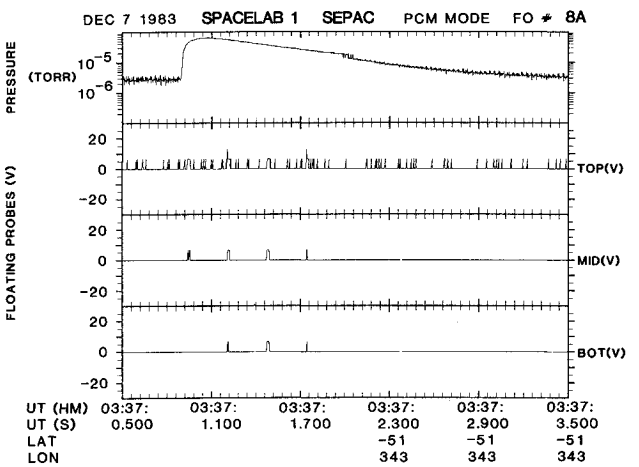

Fig. 6 Floating probe voltage data. The top panel is neutral gas pressure data, whereas the second, third, and fourth panels are the voltages monitored on the top, middle, and bottom floating probes, respectively.

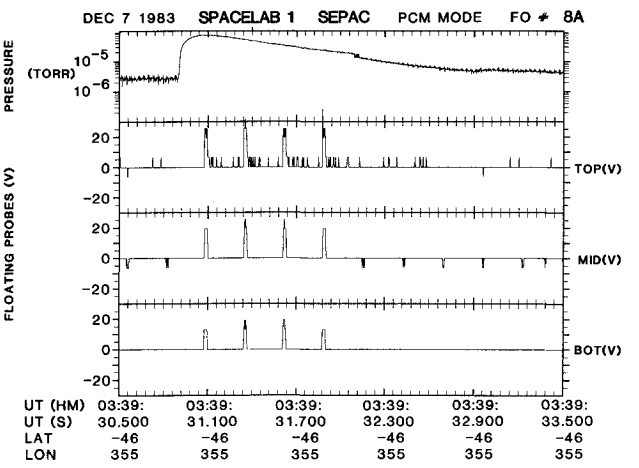

Fig. 7 Floating probe voltage data.

Summary

Table 1 gives a summary of the data from all six instances of neutral gas releases during which the PICPAB beam was fired. Table 1 lists the peak pressure during the gas release; ΔI, the difference in the peak values of the langmuir probe current before and after the gas release and the electric field strength between the bottom floating probe and the Shuttle surface. It is clear from the table that the response of the plasma diagnostics depends on the amount of gas released. All the events in class 1 have high gas pressure (70×10^{-6} Torr) and the two events in class 2 low gas pressure ($< 10 \times 10^{-6}$ Torr). For class 1 events, the langmuir probe signal shifts from positive to negative during the release ($\Delta I < 0$), and in all but one such instance, the electric field exceeds 24 mV/m in the direction away from the Shuttle. For class 2 events, both ΔI and the field are zero. There is a similar pattern in the low-frequency wave data: the larger gas releases show greater increases in intensity.

Discussion

The increase in current collected by the langmuir probe indicates that there is additional plasma created during the time of the neutral gas release. The stimulation of wave activity at the lower hybrid resonance is also indicative of enhanced ionization. This increased ionization could occur through simple collisions, or through a more disruptive mechanism such as a beam plasma discharge (BPD).

The number of ionizations per second that can be expected from collisions alone is given to good accuracy by[10]

$$\text{ionization/s} = (I_b/e)Ln\sigma$$

$$= 6.2 \times 10^{13}(P/\text{s})$$

where $L = 2$ m is the assumed length of the interaction region, $I_b = 10^{-1}$ A, P is the neutral pressure in 10^{-6} Torr, and the cross section σ is taken to be 1.5×10^{-17} cm^2 for 8 keV electrons according to Ref. 11. If, following Ref. 12, we take the plasma diffusion velocity to be 10^3 m/s, we can calculate that the newly ionized plasma will leave the 2 m active region within 2 ms. This

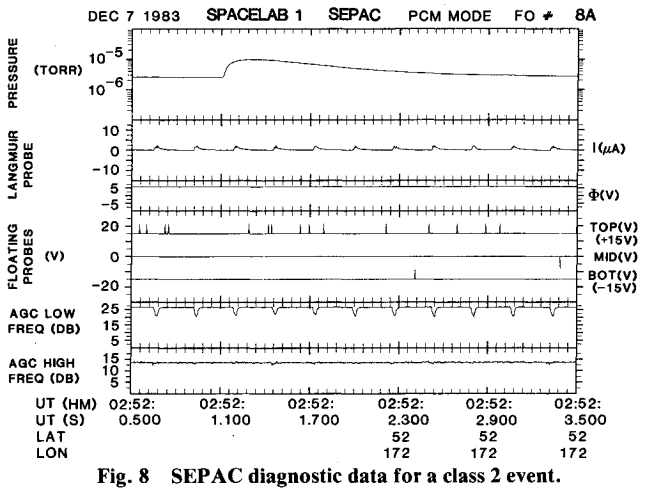

Fig. 8 SEPAC diagnostic data for a class 2 event.

Table 1 Summary of gas release data

Class	Day	UT	Pressure, 10^{-6} Torr	ΔI[a], μA	Field[b], mV/m
1	Dec. 7, 1983	3:37:00	70	−7.0	24
1	Dec. 7, 1983	3:39:30	70	−9.5	45
1	Dec. 7, 1983	2:24:30	70	−8.0	24
1	Dec. 7, 1983	2:54:31	70	−7.5	?
2	Dec. 7, 1983	2:52:00	10	0	0
2	Dec. 4, 1983	18:48:00	3.5	0	0

[a]ΔI = current (after) − current (before). [b]Field = voltage (bottom probe)/distance.

diffusion time is supported by the data: a close examination of the peaks in the langmuir probe data indicates that the current reaches its maximum within 1 or 2 ms and remains in a steady state for the duration of the 20 ms beam pulse. Given that the active region of the neutral cloud had a radius of 1 m, and integrating the ionization rate over 2 ms, one would expect plasma density increases on the order of 1.0, 3.0, and 21.0×10^5 cm^{-3} for pressures of 3.5×10^{-6} Torr, 1×10^{-5} Torr, and 7×10^{-5} Torr, respectively.

The ambient plasma density in sunlight at an altitude of 250 km is on the order of 5×10^5 cm^{-3}; thus, we can expect that the additional plasma density due to collisional ionization will be greater than the ambient plasma density in the case of the large gas releases ($P = 7 \times 10^{-5}$ Torr), but not in the cases where the neutral pressure only reaches 1×10^{-5} Torr or less. Ionization by collisions alone does then account for the additional langmuir probe current in the former case and the lack of it in the latter.

Although the additional current to the langmuir probe can be understood by collisional ionization, the sign change in the langmuir probe current with the onset of the neutral gas release is still to be explained. A negative current signal indicates that the probe is either attracting ions or emitting electrons. Both options initially seem unlikely with + 6 V applied potential. The effective collection of ions is made virtually impossible by their comparatively large mass. Electron emission can occur during an electron discharge from the probe, but a direct discharge from the probe would require at least a potential difference on the order of 1 kV between the probe and the plasma, which is much higher than indicated by the floating probes. Alternatively, a more reasonable explanation for electron emission is that the ionized plasma cloud is at a higher potential than the spacecraft and secondary electron fluxes exceed the primary incident electron fluxes. For a positive potential difference ($\phi_0 > 0$) (the spacecraft is assumed to be at zero potential), primary incident electrons are decelerated and secondary electrons escape. When secondary electron fluxes exceed incident fluxes at the probe surface, the langmuir probes will measure a negative current signal. When $\phi_0 < 0$, incident electrons are accelerated and secondary electron fluxes always exceed incident fluxes; however, the langmuir probe will not record a negative current signal since secondary electrons cannot escape and will form a sheath around the probe in an equilibrium. In fact, the floating probes confirm the existence of such a positive potential gradient. Recalling Fig. 6 and Table 1, we calculate a + 24 V/m gradient between the bottom probe and the spacecraft.

The conditions under which the secondary electron flux J_{sec} is greater than the primary flux J_{inc} for a positive potential difference ϕ_0 between the probe and the ionized gas cloud were investigated. The electron distribution in the plasma cloud is assumed to be an isotropic Maxwellian function $f(E)$ before passing through the potential. At the probe surface, the distribution function is then $f(E + e\phi_0)$. The primary and secondary electron fluxes are then given by [13]

$$J_{inc} = 2\pi \int_0^\infty dv v^3 f(E + e\phi_0) \tag{1}$$

$$J_{sec} = 2\pi \int_0^\infty dv \int_0^{\pi/2} d\theta v^3 \cos\theta \sin\theta f(E + e\theta_0)\delta(E,\theta) \tag{2}$$

where $E = m_e v^2/2$ is the electron energy at the probe surface. The factor $\delta(E, \theta)$ is the yield of secondary electrons defined as the average number of emitted electrons per incident electron with an incident energy E and an angle of incident θ relative to the surface normal. The energy and angle dependence of the secondary electron yield $\delta(E,\theta)$ is given in Ref. 13.

With Eqs. (1) and (2), a numerical integration was done to calculate the primary and secondary electron fluxes incident on gold as a function of the potential energy gained by an electron passing through the potential drop ϕ_0. Figure 9 shows the ratio of incident and secondary fluxes plotted against ϕ_0 for electron

temperature T = 100 eV, 150 eV, and 200 eV. These plots show that only for incident electron temperatures greater than 150 eV will secondary flux be greater than incident flux ($J_{sec}/T_{inc} > 1$) for $\phi_0 > 0$. For a potential difference of about 10 V as measured by the floating probe, an electron temperature of 150 eV or greater is required. For an electron temperature of 200 eV, a potential difference between the probe and the plasma can be less than 100 eV in order for the secondary flux to exceed the incident flux.

Although there is no measurement of the electron energy spectrum for energy greater than 150 eV from the SEPAC DGP, an enhancement in the electron flux at 100 eV is observed by the EPA. Preliminary uncalibrated data from one of the electrostatic analyzers on the low-energy electron spectrometer and magnetometer experiment (IES-019A) on Spacelab (see Ref. 14 for a description of the experiment) do show an enhancement of flux in the 200 to 400 eV range (K. Wilhelm, private communication, 1988). Therefore, our suggestion of a hot plasma cloud is consistent with the available plasma data.

In summary, the langmuir probe and floating probe data indicate that the Shuttle appears to be at a lower potential than the ambient plasma after having emitted electrons in a beam firing. One explanation of the anomalous charging phenomenon is that there is a region of hot dense plasma in the immediate area of the payload bay, formed as a result of the ionization of the neutral Argon gas released from the MPD.

Computer Simulation

The existence of a positive potential gradient between the newly created plasma cloud in the payload bay and the Orbiter seems to explain the data from the plasma probes; a computer simulation using a particle-in-cell (PIC) electrostatic code was conducted to determine whether such a gradient might, in fact, develop under the given conditions. A one-dimensional model was used to represent the system with the spatial direction taken to be the direction of the magnetic field. The simulation initially has two electron components, a cold uniform component filling the entire system and a finite width slab of hot electron plasma. The slab of hot electrons models those produced by the interactions of the electron beam and the neutral gas. The simulation model assumes that the ions in the background plasma have the same locations as the cold and hot electrons so that the net charge density is zero everywhere initially. The ions are assumed to be motionless because of their heavy mass.

The thermal speed within the hot electron slab a_h is taken to be $0.01c$, and the thermal speed of the uniform cold electrons is taken to be $0.001c$, where c is the speed of light, the unit of velocity used in the simulations. In terms of temperature T_h, the thermal speed a_h is defined as $\sqrt{T_h/2m_e}$, where m_e is the electron mass. We used 4096 particles for the hot electron slab and 8192 particles for the cold component. Because the hot component is distributed over one-quarter of the simulation system, the number density of the hot component is twice that of the cold component. The simulation system is subdivided into 64 cells. The simulation system has a length L of $7.2\,c/\omega_{pe}$, where ω_{pe} is the electron plasma frequency inside the hot electron slab. The system length L is approximately equal to 500 λ_D, where $\lambda_D = a_h/\sqrt{2}\omega_{pe}$ is the electron Debye length for the hot electrons.

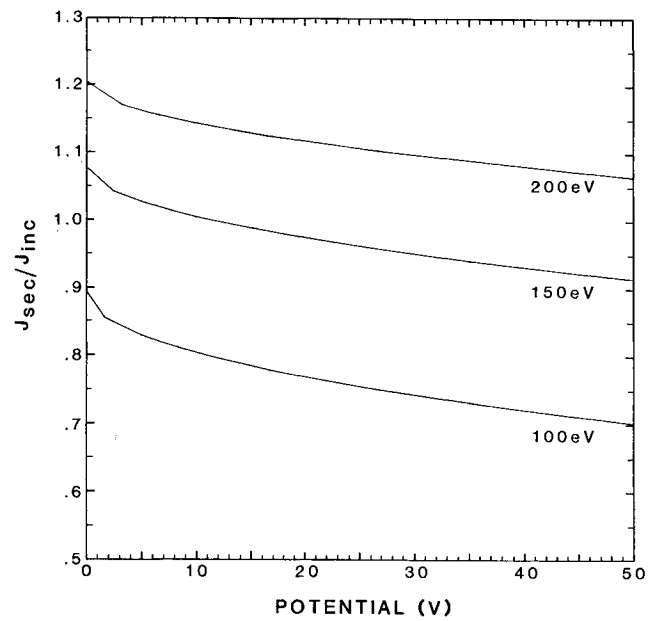

Fig. 9 Ratio of secondary electron flux to incident flux vs ϕ_0 for electron temperature T = 100 eV, 150 eV, and 200 eV.

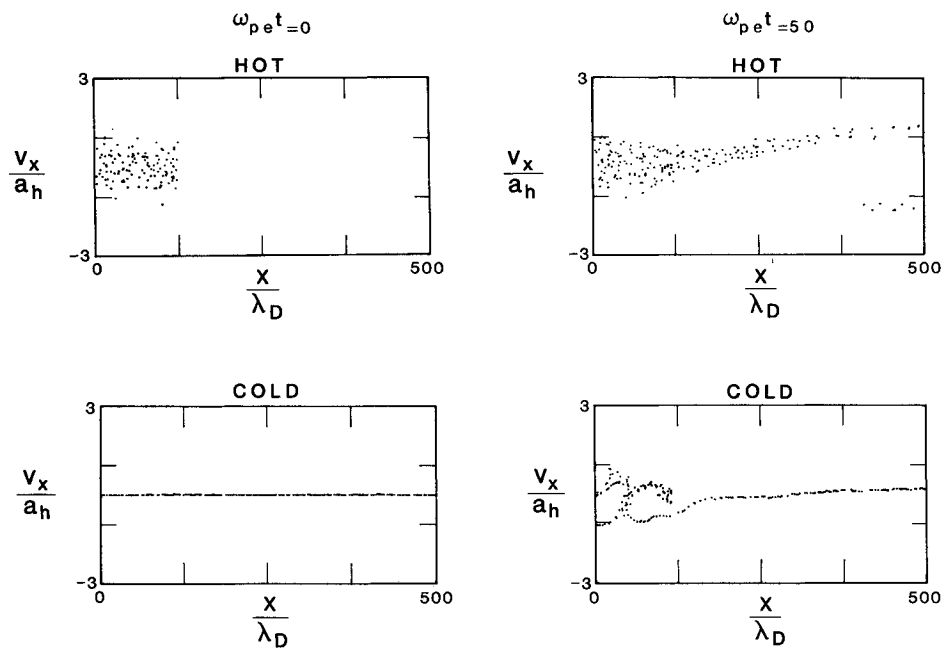

Fig. 10 Phase space plot of the simulated spacecraft-plasma system for the initial configuration (left panels) and the configuration at a later time (right panels). The vertical coordinate is velocity normalized by the thermal speed of the hot electrons, and the horizontal coordinate is distance normalized by the Debye length of the hot electrons.

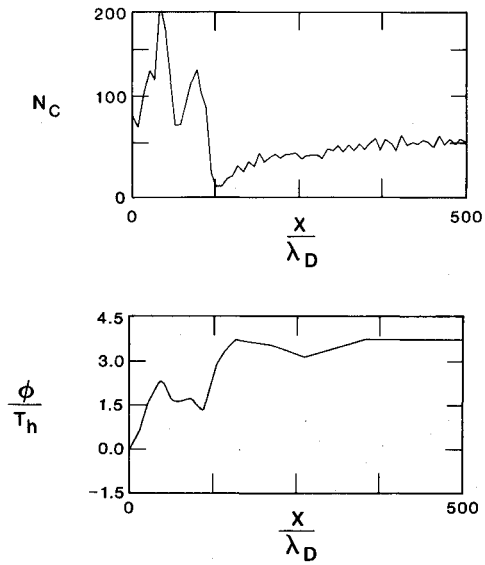

Fig. 11 Number of cold electrons per cell N_c (top) and potential (bottom) as computed in the simulation. The potential is normalized by the hot electron temperature.

In the specified parameters, we initialize the simulations by loading the particles uniformly in space and assigning them random velocities such that Maxwellian distributions are produced. The hot electron slab is loaded from $x = 0$ to $x = L/4$. The $v_x - x$ phase space plot of the initial system is shown in the left two panels of Fig. 10 for the hot component (top) and the cold component (bottom). The system is then allowed to evolve in time. The spacecraft is assumed to be positioned at the left-hand boundary $x = 0$, so that the potential is zero and particles leaving that boundary are reflected. The electric field is assumed to be zero at the $x = L$ boundary in solving Poisson's equation. The simulation is stopped at about time $t = 50\omega_{pe}$ when hot electrons are just reflected from the right-hand boundary. The phase space plots near the end of the simulation runs are shown in the right-hand panels.

The right-hand panels of Fig. 10 show that at 50 ω_{pe}, the hot electrons have escaped from the slab, and the cold electrons have bunched toward the origin, forming a space charge separation. Figure 11 shows a plot of the number of cold electrons per cell (top) and potential (bottom) vs distance. The number of cold electrons per cell is enhanced within the left quarter of the system and depressed in the second quarter. The potential double layer is clearly in evidence with a positive potential gradient between $x = 0$ and $x = L/4$. The total potential drop of the double layer is about four times that of the hot electron temperature. It is this double-layer structure that allows the secondary electrons to escape from the langmuir probe, yielding a net negative current.

Conclusions

Based on the evidence of the simulation and the secondary electron production calculations, it seems that the formation of a double-layer structure separating a hot plasma cloud from the cold ambient plasma is a reasonable scenario. The hot plasma cloud is probably produced by the ionization of the released neutral gas. The anomalous signatures of spacecraft charging potential and return current observed by the SEPAC diagnostic instruments imply that the electron temperature of the hot plasma cloud is greater than 150 eV. Further detailed studies of plasma data are needed to confirm the existence of such a hot electron cloud. Finally, there appears to be no direct evidence for beam plasma discharge (BPD), and the experimental results can be explained without evoking such a discharge.

Acknowledgments

This research was supported by NASA Contract NAS8-32488 and Air Force Geophysical Laboratory Contract F19628-85-K-004. The authors would like to thank William Bernstein, Susumu Sasaki, and Bill Taylor for useful discussions, and Ron Williams and Jill Johnson for their assistance in data analysis. We would further like to thank Klaus Wilhelm and Colin Barrow of the Max Plank Institute für Aeronomie for providing additional electron energy analyzer data from Spacelab 1. We acknowledge the San Diego Supercomputer Center for the use of the CRAY X-MP.

References

[1]Obayashi, T., Kawashima, N., Kuriki, K., Nagatomo, M., Ninomiya, K., Sasaki, S., Yanagisawa, M., Kudo, I., Ejiri, M., Roberts, W. T., Chappell, C. R., Reasoner, D. L., Burch, J. L., Taylor, W. L., Banks, P. M., Williamson, P. R., and Garriot, O. K., "Space Experiments with Particle Accelerators," *Science,* Vol. 225, July 1984, pp. 195, 196.

[2]Beghin, C., Lebreton, J. P., Maehlum, B. N., Troim, J., Ingsoy, P., and Michau, J. L., "Phenomena Induced by Charged Particle Beams," *Science*, Vol. 225, July 1984, pp. 188-191.

[3]Ingsoy, P., Maehlum, B. N., Troim, J., and Lebreton, J. P., "Plasma Energization in the Shuttle Wake Region During Beam Injection from Spacelab 1," *Planet Space Science*, Vol. 34, June 1986, pp. 555-562.

[4]Katz, I., Jongeward, G. A., Parks, D. E., Reasoner, D. L., and Purvis, C. K., "Energy Broadening Due to Space Charge Oscillations in High Energy Electron Beams," *Geophysical Research Letters*, Vol. 13, Jan. 1986, pp. 64-67.

[5]Neubert, T., Taylor, W. W. L., Storey, L. L. R. O., Kawashima, N., Roberts, W. T., Reasoner, D. L., Banks, P. M., Gurnett, D. A., Williams, R. L., and Burch, J. L., "Waves Generated During Electron Beam Emissions from the Space Shuttle," *Journal of Geophysical Research*, Vol. 91, Oct. 1986, pp. 11,321-11,330.

[6]Cai, D., Sasaki, S., and Abe, K., "Extremely Low Frequency Oscillations Excited by Electron Beam Injection in SEPAC Spacelab 1 Experiment," Institute of Space and Astronautical Science, Tokyo, Japan, ISAS Res. Note 298, 1985.

[7]Katz, I., Mandell, J. J., Jongeward, G. A., and Lilley, J. R., Jr., "Astronaut Charging in the Wake of a Polar Orbiting Shuttle," *Proceedings of the AIAA Shuttle Environment and Operations II Meeting*, AIAA, New York, 1985.

[8]Sasaki, S., Kawashima, N., Kuriki, K., Yanagisawa, M., and Obayashi, T., "Vehicle Charging Observed in SEPAC Spacelab 1 Experiment," *Journal of Spacecraft and Rockets*, Vol. 23, March-April 1986, pp. 194-199.

[9]Sasaki, S., Kawashima, N., Kuriki, K., Yanagisawa, M., Obayashi, T., Roberts, W. T., Reasoner, D. L., Taylor, W. W. L., Williamson, P. R., Banks, P. M., and Burch, J. L., "Ignition of Beam Plasma Discharge in the Electron Beam Experiment in Space," *Geophysical Research Letters*, Vol. 12, Oct. 1985, pp. 647-650.

[10]Kellogg, P. J., Anderson, H. R., Bernstein, W., Hallinan, T. J. Holzworth, H. R., Jost, R. J., Leinbach, H., and Szuszuczewicz, E. P., "Laboratory Simulation of Injection Particle Beams in the Ionosphere," *Artificial Particle Beams in Space Plasma Studies*, edited by Bjorn Grandal, 1982, pp. 289-329.

[11]Tawara, H., Kato, T., and Ohnishi, M., "Ionization Cross Sections of Atoms and Ions by Electron Impact," Institute of Plasma Physics, Nagoya Univ., Nagoya, Japan, IPPJ-AM-3, Feb. 1985, p. 117.

[12]Sasaki, S., Kawashima, N., Kuriki, K., Yanagisawa, M., Obayashi, T., Roberts, W. T., Reasoner, D. L., Taylor, W. W. L., Williamson, P. R., Banks, P. M., and Burch, J. L., "Gas Ionization Induced by a High Speed Plasma Injection in Space," *Geophysical Research Letters*, Vol. 13, May 1986, pp. 434-437.

[13]Laframboise, J. G., "The Threshold Temperature Effect in High-Voltage Spacecraft Charging," *Proceedings of AFGL Workshop on Natural Charging at Large Space Structures in Near Earth Polar Orbit*, Air Force Geophysics Lab., Wright-Patterson AFB, OH, 1983, pp. 293-308.

[14]Wilhelm, K., Studemann, W., and Riedler, W., "Electron Flux Intensity Distributions Observed in Response to Particle Beam Emissions," *Science*, Vol. 225, July 1984, pp. 195, 196.